

Detection of Lesions in Lettuce Caused by *Pectobacterium carotovorum* Subsp. *carotovorum* by Supervised Classification Using Multispectral Images

Glecia Júnia dos Santos Carmo, Renata Castoldi, George Deroco Martins, Ana Carolina Pires Jacinto, Nilvanira Donizete Tebaldi, Hamilton César de Oliveira Charlo & Renan Zampiroli

To cite this article: Glecia Júnia dos Santos Carmo, Renata Castoldi, George Deroco Martins, Ana Carolina Pires Jacinto, Nilvanira Donizete Tebaldi, Hamilton César de Oliveira Charlo & Renan Zampiroli (2022) Detection of Lesions in Lettuce Caused by *Pectobacterium carotovorum* Subsp. *carotovorum* by Supervised Classification Using Multispectral Images, Canadian Journal of Remote Sensing, 48:2, 144-157, DOI: [10.1080/07038992.2021.1971960](https://doi.org/10.1080/07038992.2021.1971960)

To link to this article: <https://doi.org/10.1080/07038992.2021.1971960>



Published online: 21 Oct 2021.



Submit your article to this journal [↗](#)



Article views: 130



View related articles [↗](#)



View Crossmark data [↗](#)



Detection of Lesions in Lettuce Caused by *Pectobacterium carotovorum* Subsp. *carotovorum* by Supervised Classification Using Multispectral Images

Détection de lésions sur la laitue par *Pectobacterium carotovorum*, sous-espèce *carotovorum*, au moyen d'une classification supervisée d'images multispectrales

Glecia Júnia dos Santos Carmo^a , Renata Castoldi^a , George Deroco Martins^b , Ana Carolina Pires Jacinto^c , Nilvanira Donizete Tebaldi^c , Hamilton César de Oliveira Charlo^d , and Renan Zampiroli^a 

^aInstituto de Ciências Agrárias, Universidade Federal de Uberlândia, Monte Carmelo, Brazil; ^bDepartamento de Engenharia Civil (FECIV), Universidade Federal de Uberlândia, Monte Carmelo, Brazil; ^cInstituto de Ciências Agrárias, Universidade Federal de Uberlândia, Uberlândia, Brazil; ^dInstituto Federal de Educação, Ciência e Tecnologia do Triângulo Mineiro, Uberaba, Brazil

ABSTRACT

This study aimed to detect soft rot caused by *Pectobacterium carotovorum* subsp. *carotovorum* in lettuce using images obtained by multispectral sensors mounted on an unmanned aerial vehicle (UAV). A secondary objective was to identify the best sensor and determine the optimal stage after inoculation to detect infected plants. In the field, soft rot lesions and the agronomic traits of lettuce plants inoculated or not with the bacteria were assessed on different days after inoculation (DAI). Classifications were made using the Support Vector Machine (SVM) and Naive Bayes (NB) algorithms to analyze data groups consisting of spectral bands, vegetation indices and a combination of bands and indices obtained from a conventional visible camera and Mapir Survey3W multispectral camera, as well as agronomic parameters. The results confirmed the possibility of pre-symptomatic detection of *P. carotovorum* subsp. *carotovorum* in lettuce at the canopy level. With respect to identifying healthy and infected lettuce plants by supervised classification, the best results were obtained at 4 and 8 DAI, especially when using the subsets derived from the Mapir Survey3W camera (RGN sensor), for both classifiers. The subsets obtained with the conventional visible sensor (RGB sensor) produced the best results at 20 and 24 DAI.

RÉSUMÉ

Cette étude a pour objectif de détecter la pourriture molle causée par *Pectobacterium carotovorum*, sous-espèce *carotovorum*, sur la laitue à l'aide d'images prises par des capteurs multispectraux montés sur un drone (UAV). De plus, un objectif secondaire est d'identifier le meilleur capteur et la meilleure phase après l'inoculation pour détecter les plantes infectées. Au champ, les lésions de pourriture molle et les paramètres agronomiques des plants de laitue inoculés ou non avec la bactérie ont été évalués plusieurs jours après l'inoculation (DAI). Pour les classifications, les algorithmes Support Vector Machine (SVM) et Naive Bayes (NB) ont été utilisés pour évaluer des groupes de données composés de bandes spectrales, d'indices de végétation et de combinaison de bandes et d'indices obtenus à partir d'une caméra visible conventionnelle et d'une caméra multispectrale Mapir Survey3W, ainsi que les paramètres agronomiques. Les résultats ont confirmé la possibilité d'une détection pré-symptomatique de *P. carotovorum*, sous-espèce *carotovorum* dans la laitue au niveau de la canopée. Pour la détection de plants de laitue sains et infectés par classification supervisée, les meilleurs résultats ont été obtenus à 4 et 8 jours après l'inoculation (DAI), principalement en utilisant des sous-ensembles dérivés de la caméra Mapir Survey3W (capteur RVIR), pour les deux classificateurs. Alors que, les sous-ensembles dérivés du capteur visible conventionnel (capteur RVB) ont montré les meilleurs résultats aux intervalles de 20 et 24 jours après l'inoculation.

ARTICLE HISTORY

Received 10 February 2021
Accepted 13 August 2021

Introduction

Lettuce (*Lactuca sativa*) is the most economically important leafy vegetable worldwide. In Brazil, the number of growers and volume produced continues to rise (Anuário Brasileiro de Horti&Fruti 2020 2019).

However, a number of pathogens that affect plants from the root system to leaves can drastically reduce crop yields. Nazerian et al. (2013) found that more than 15% of the damage observed in lettuce in the field, greenhouses and storage was caused by bacteria from the genus *Pectobacterium* spp.

Pectobacterium carotovorum subsp. *carotovorum*, the causal agent of soft rot, is considered one of the ten most scientifically and economically important phyto-bacteria (Mansfield et al. 2012); however, there are no chemical products for its control registered in Brazil or resistant varieties (Agrofit 2020).

The initial symptoms of the disease are wilting and depigmentation of the older leaves. A brownish green water-soaked lesion then develops in the inner stem, which may progressively cause the entire plant to rot (Colariccio and Chaves 2017), resulting in yield and economic losses for producers. Initial symptoms are difficult to see and, when observed, almost impossible to control. As such, any strategy aimed at detecting these anomalies in the early stages of development is vitally important, since the disease is aggressive and the growth cycle of lettuce short.

Remote sensing (RS) has a number of applications in agriculture (Weiss et al. 2020). A review by Usha and Singh (2013) cites several potential applications for RS, including disease detection in crops such as tomato, beet, cucumber and potato; measuring canopy volume in tomato; estimating area and obtaining production information in potato and cabbage.

The development and applications of RS for agriculture is due to knowledge of leaf and canopy reflectance, which makes it possible to calculate vegetation indices and, consequently, assess agronomic traits such as nutritional status, biomass, leaf area, and water stress (Hatfield et al. 2008), in addition to helping detect and monitor plant disease (Gogoi et al. 2018).

Several papers have reported the use of different sensors, such as multi- and hyperspectral reflectance sensors, RGB imaging, thermography and fluorescence sensors, among others, to study diseases. They can be installed on different platforms, including unmanned aerial vehicles (UAVs) (Mahlein 2016; Maes and Steppe 2019; Oerke 2020). However, according to Mahlein (2016), there are still no sensors on the market to specifically detect diseases in plants, since the

full potential of sensor-based detection has yet to be explored. In this respect, the present study aimed to determine the most promising sensor for the disease analyzed.

In conjunction with RS, machine learning has been widely used in agriculture through learning models such as classification, regression, clustering, Bayesian and instance-based models, decision trees, artificial neural networks and support vector machines (Liakos et al. 2018). Thus, data processing using machine learning can contribute to identifying diseases in melon (Pineda et al. 2018) and sugar beet (Ozguven and Adem 2019), separating healthy from sick leaves in pepper (Karadag et al. 2018) and potato plants (Fernández et al. 2020), investigating in potato plants late blight physiological differences (Gold et al. 2020), and early detection and classification of tomato virus (Morellos et al. 2020).

In lettuce cultivation, algorithms have been used to detect iron, zinc and nitrogen deficiency (Hetzroni et al. 1994), assess chlorophyll content (Odabas et al. 2017), estimate nitrogen content (Jun et al. 2013, Mao et al. 2015, Gao et al. 2015), determine the nutritional status of plants under different irrigation and fertilization conditions (Ren et al. 2017), analyze the effect of water stress (Kizil et al. 2012), measure pesticide residues (Sun et al. 2018), spectral determination of cadmium (Xin et al. 2020), and identify and assess microbial contamination (Rahi et al. 2020).

However, there are no studies on the use of RS and/or machine learning to identify stem and root diseases that affect lettuce crops, making it essential to obtain and apply tools capable of early detection, since this allows disease to be controlled and minimizes economic losses.

As such, this study aimed to detect soft rot caused by *Pectobacterium carotovorum* subsp. *carotovorum* in lettuce using images obtained by multispectral sensors mounted on an unmanned aerial vehicle (UAV), identify the best sensor and determine the optimal stage after inoculation to detect sick plants based on the multispectral images.

Material and methods

Field experiment

The experiment was conducted at the Federal University of Uberlândia (UFU), Monte Carmelo Campus (geographic coordinates: 18° 43' 26.77271" S, 47° 31' 25.66202" W, and altitude of 912.469 m). According to Köppen's classification system, climate

in the region is wet and temperate, with hot summers and dry winters (Embrapa 2006).

The crispy endive lettuce cultivar ‘Solaris’[®], classified as susceptible to *Pectobacterium carotovorum* subsp. *carotovorum* isolates, was used (Félix et al. 2014).

Seeds were planted in 200 cell expanded polystyrene trays filled with commercial pine bark-based substrate. The seedlings were kept in a greenhouse covered in clear UV-resistant plastic (150 micra) and irrigated daily to ensure the substrate was always moist, which is ideal for seedling development.

At 25 days after planting (DAP), the seedlings were transplanted to five-liter plastic pots filled with soil, and initially maintained in a greenhouse under shade cloth. The soil used was collected from a ravine area, sieved, limed and fertilized, in accordance with soil analysis and crop recommendations (Fontes 1999).

The *Pectobacterium carotovorum* subsp. *carotovorum* isolate UFU A7, supplied by the Plant Bacteriology Laboratory (LABAC) of the Federal University of Uberlândia, was used for inoculation. The isolate was grown in bacteria screening medium 523 (Kado and Heskett 1970) for 24 h at 28 °C. The bacterial suspension was prepared in filtered water and adjusted in a spectrophotometer to $A_{570} = 1.8$ (5×10^9 UFC mL⁻¹).

At 27 days after transplanting (DAT), 196 plants were inoculated with 100 µl of the bacterial suspension in the central stem region, using a disposable 1 mL syringe. After inoculation, the plants were placed in plastic bags in a humidity chamber, for 12 hours. The same number of plants (196) were not inoculated and considered healthy plants for the duration of the experiment.

Disease lesions were assessed at 4, 8, 12, 16, 20, 24 and 28 days after inoculation (DAI) using the rating scale proposed by Ren et al. (2001), with adaptations. Scores ranged from 1 to 8, whereby 1 = no lesions at the inoculation site; 2 = lesions smaller than 5 mm, 3 = lesions between 5 and 10 mm, 4 = lesions larger than 10 mm, but not reaching the leaves near the inoculation site, 5 = lesions larger than 10 mm,

reaching the leaves near the inoculation site, 6 = lesions larger than 10 mm, reaching leaves near and far from the inoculation site, 7 = whole plant near death, 8 = dead plant.

Agronomic assessments were performed in 392 plants, at the same intervals described above. At each interval, 28 inoculated and non-inoculated plants were evaluated to determine the chlorophyll index, using an electronic chlorophyll meter (ClorofiLOG Falker CFL1030), as well as plant fresh mass (kg), stem length (cm), stem diameter (cm) and fresh root mass (kg).

The plants were irrigated every day in the morning and afternoon to maintain soil moisture content close to field capacity, the ideal condition for disease development.

Image capturing and processing

In order to obtain the images, the plants were relocated to an area outside the greenhouse. The soil was covered in black plastic (Figure 1) and the plants protected by black 40–45% shade cloth, installed 2.0 m above the ground.

On the same days as the agronomic assessments (4, 8, 12, 16, 20, 24 and 28 days after inoculation), flights were made over the area between 12 and 1 p.m. (period with the most sunlight), during which the shade cloth was removed (Figure 1) so as not to interfere with the images.

The images were obtained by a Phantom 4 Pro unmanned aerial vehicle (UAV) or drone, made by DJI (Dà-Jiāng Innovations Science and Technology Co.), equipped with a conventional visible camera with channels corresponding to the red (650 nm), green (550 nm) and blue (480 nm) (RGB) bands, full width at half maximum (FWHM) of 10 nm and 20 megapixel resolution, as well as a Mapir Survey3W camera with 12 megapixel resolution, channels corresponding to the red (660 nm), green (550 nm) and near infrared (850 nm) (RGN) bands and FWHMs of 40, 60 and 80 nm, respectively.



Figure 1. Arrangement of the plants studied.

All the flights were planned using DroneDeploy[®] software, which established 5 bands, an altitude of 20 meters, speed of 2 m/s, front and side overlap of 75 and 70%, respectively, and a flight time of approximately 4 min.

After images were captured by the RGB and RGN sensors, mosaicking was performed for each of the seven flights, using AgisoftPhotoScan Professional software. This software aligns the images to find the ideal camera position and common points to combine them, forming a sparse point cloud. A dense point cloud was then constructed, based on which the surface was generated using a 3D polygon mesh, producing mosaics for each flight.

Radiometric calibration was carried out using Mapir Camera Control (MCC) software, only for the seven mosaics generated based on the Mapir Survey3W images. To that end, before each flight the camera photographed the calibration target, which had four color bands (black, dark gray, light gray and white) of known radiance. The model, lens and filter of the Mapir Survey3W camera used were specified in the software, the target image of the respective flight selected and the QR code of the target detected. This made it possible to calculate the calibration values needed for the camera, and each input file containing the mosaic was loaded. After calibration, the calibrated mosaic file was automatically created.

Given that the radiances of objects may vary over time and because the present study uses temporal images, radiometric normalization of both the RGB (digital number) and RGN (reflectance) mosaics was carried out for spectral characterization, in accordance with Hall et al. (1991).

The image from the last flight was used as reference in normalization because of its higher solar radiation. For all of the flights, the calibration target of the Mapir Survey3W camera (Figure 2) was positioned in the overflown area and thereby used to extract the means of the light and dark pixel sets for all the images, since the target's radiance is stable.

The mean values of the digital numbers and reflectances for the dark and light pixel sets in the red (R), green (G), blue (B) and near-infrared bands (N) (RGB and RGN bands) were manually extracted from the reference image and other images.

Next, the following equation was used to determine the coefficients of a linear transformation (Ponzoni et al. 2012):

$$Ti = mi \times xi + bi \quad (1)$$

where:

$$mi = \frac{Bri - Dri}{(Bsi - Dsi)} \quad (2)$$

$$bi = \frac{Dri \times Bsi - Dsi \times Bri}{(Bsi - Dsi)} \quad (3)$$

Ti = Digital number (RGB) and reflectance (RGN) of the reference image; xi = Digital number (RGB) and Reflectance (RGN) of the image to be normalized; Bri = mean of the light reference set; Dri = mean of the dark reference set; Bsi = mean of the light set to be normalized; Dsi = mean of the dark set to be normalized and i = sensor bands studied.

In ENVI 5.1 (Environment for Visualizing Images) software and using the Band Math tool, the equation was applied to each image band, producing layers. The three layers generated for each image were combined into a single image with values similar to those of the reference image.

The radiometric data (mean values of the digital numbers and reflectances in the RGB and RGN bands, respectively) of the 28 inoculated and 28 non-inoculated plants were extracted from each mosaic, using the region of interest (ROI) function in ENVI 5.1 software.

Calculating the vegetation indices

The mean spectral values of healthy lettuces and those inoculated with the bacteria were used to calculate the vegetation indices in the visible and near-infrared (NIR) spectra (Table 1), which are sensitive to biophysical and biochemical variations in plants.

Supervised classification

In order to differentiate between healthy and infected lettuces, supervised classification was performed based on the Naive Bayes (NB) probabilistic algorithm and support vector machine (SVM) nonparametric classifier, defined as an SMO (Sequential Minimal Optimization) algorithm, implemented in Weka 3.9.4 software (Waikato Environment for Knowledge Analysis). Both classifiers have been used in previous studies involving plant diseases (Tetila et al. 2017; Mondal et al. 2017; Poblete et al. 2020; Abdu et al. 2020).

There are several applications of SVMs in remote sensing (Mountrakis, Im and Ogole 2011). The input data are nonlinearly mapped into a high-dimensional



Figure 2. Calibration target of the Mapiir Survey3W camera to extract the mean values of dark and light pixel sets.

space, where the support vectors define a hyperplane, making the data linearly separable (Cortes and Vapnik 1995). To that end, the PUK (Pearson VII universal kernel) function with Sigma (σ) = 1, Omega (ω) = 1 and penalty parameter $C=1$ were used, after previous tests. On the other hand, Naive Bayes learning is based on the Bayes' theorem, which assumes features to be independent and calculates the probabilities of their belonging to different classes (Berrar 2018).

Inserted into the input dataset were the classes obtained in the assessment, mean values of the digital numbers and reflectances of the RGB and RGN bands, respectively, the vegetation indices calculated and agronomic variables analyzed.

For classification in Weka software, the non-inoculated (healthy) plants were considered class 0 and all the infected plants, with their different levels of disease obtained in the field, class 1.

The subsets selected for classification at each assessment time were as follows: 1- only bands (for each camera), 2- only indices and 3- bands and indices combined. The agronomic variables were classified separately to compare with the image-based classifications. Each subset was classified using 70% of the data for training and 30% for testing, for both SVM and NB. Therefore, it should be noted that for the validations of the various classifications, 20 training and 8 validation samples were used for each class. It is

Table 1. Vegetation indices calculated based on wavelengths of the visible (R, G and B) and near-infrared (NIR) spectra of lettuce inoculated or not with *Pectobacterium carotovorum* subsp. *carotovorum*.

Vegetation Index	Equation	Application	Reference
Normalized Green Red Difference Index	$NGRDI = \frac{(B_{550} - B_{650})}{(B_{550} + B_{650})}$ (4)	Leaf area index (LAI), biomass	(Tucker 1979; Hunt et al. 2005)
Carotenoid Reflectance Index 1	$CRI1 = \frac{(1)}{(B_{480})} - \frac{(1)}{(B_{550})}$ (5)	Carotenoid content	(Gitelson et al. 2002)
Photochemical Reflectance Index	$PRI = \frac{(B_{480} - B_{550})}{(B_{480} + B_{550})}$ (6)	Photosynthesis efficiency	(Gamon et al. 1992; Garbulsky et al. 2011)
Triangular Greenness Index	$TGI = B_{550} - 0.39 \times B_{650} - 0.61 \times B_{480}$ (7)	Chlorophyll, Nitrogen management, Canopy area	(Hunt et al. 2011; Mckinnon and Hoff 2017; Starý et al. 2020)
Green Leaf Index	$GLI = \frac{(2 \times B_{550} - B_{650} - B_{480})}{(2 \times B_{550} + B_{650} + B_{480})}$ (8)	Biomass	(Louhaichi et al. 2001; Ballesteros et al. 2018)
Normalized Difference Vegetation Index	$NDVI = \frac{(B_{850} - B_{660})}{(B_{850} + B_{660})}$ (9)	Biomass, LAI, yield and photosynthetically active radiation	(Rouse et al. 1973; Wiegand et al. 1991; Zarate-Valdez et al. 2012)
Simple Ratio	$SR = \frac{B_{850}}{B_{660}}$ (10)	Chlorophyll, LAI	(Jordan 1969)
Green Normalized Difference Vegetation Index	$GNDVI = \frac{(B_{850} - B_{550})}{(B_{850} + B_{550})}$ (11)	Chlorophyll, LAI, biomass, absorbed N and yield	(Gitelson et al. 1996; Hunt et al. 2010; Moges et al. 2005)
Difference Vegetation Index	$DVI = B_{850} - B_{660}$ (12)	Biomass, LAI	(Tucker 1979; Díaz and Blackburn 2003)
Modified Chlorophyll Absorption Reflectance Index 1	$MCARI1 = 1.2 \times [2.5 \times (B_{850} - B_{660}) - 1.3 \times (B_{850} - B_{550})]$ (13)	Greater sensitivity to LAI and less to chlorophyll	(Haboudane et al. 2004)

Monte Carmelo, 2020.

RGB sensor channels: red (B_{650}), green (B_{550}) and blue (B_{480}). RGN sensor channels: red (B_{660}), green (B_{550}) and near-infrared (B_{850}).

acknowledged that this is lower than optimal in terms of validation sample sizes, and therefore makes the classification results more sensitive to being over-estimated and under-estimated, e.g., the various results at OA 100% $k=1$, while other results are likely lower in magnitude compared to what would be expected with larger validation sample sizes. It is also noted that the term “accuracy” in this paper refers to classification agreements amongst these various smaller sample size validation sets, and therefore should not be interpreted as direct accuracy estimates.

The performance of the algorithms was evaluated using overall accuracy (OA), calculated by the ratio between correctly classified observations and the Kappa coefficient (Equation 14), which was also used by Wang et al. (2020a).

$$Kappa = \frac{\pi_0 - \pi_e}{1 - \pi_e} \quad (14)$$

Where π_0 is an observational probability of agreement and π_e a hypothetical expected probability of agreement.

Prior to classification, the mean values of the spectra were analyzed and the spectra deemed most decisive were graphically illustrated based on those obtained from infected and healthy canopies.

Results

After prior analysis of the mean spectra for the different assessment times, those obtained from the

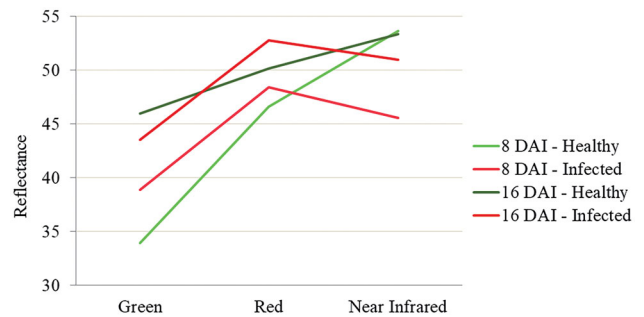


Figure 3. Spectral behavior of healthy and infected lettuce plants, calculated from mean spectrum acquired over infected and healthy canopies as a function of the number of days after inoculation (DAI).

multispectral sensor at 8 and 16 DAI for infected and non-infected plants (Figure 3) were prioritized. At 8 DAI, plants had not yet displayed visible symptoms of the disease, making agronomic intervention possible without compromising the crop; and at 16 DAI initial symptoms were visible, with plants exhibiting an intermediate level of damage.

Analysis of the behavior of spectra for healthy and infected plants at 8 DAI showed a greater difference between near-infrared reflectance values (Figure 3), demonstrating that cell structures in these two conditions differ and are decisive in differentiating between spectra, evident in the behavior observed for multispectral classification (Table 2). However, this was not possible with the RGB camera for the same period

Table 2. Supervised classification of healthy and infected plants at different assessment times.

Subsets classified	4 DAI				8 DAI				12 DAI				16 DAI			
	SVM		NB		SVM		NB		SVM		NB		SVM		NB	
	OA	K	OA	K	OA	K	OA	K	OA	K	OA	K	OA	K	OA	K
RGN	88.24	0.77	88.24	0.77	100	1	100	1	82.35	0.65	76.47	0.53	64.71	0.28	64.71	0.29
Indices	94.12	0.88	94.12	0.88	82.35	0.64	82.35	0.64	70.59	0.40	64.71	0.27	52.94	0.05	58.82	0.17
RGN and indices	100	1	100	1	100	1	94.12	0.88	76.47	0.53	76.47	0.53	58.82	0.17	58.82	0.17
R, N, NDVI, SR, GNDVI	100	1	100	1	94.12	0.88	88.24	0.76	58.82	0.17	64.71	0.28	58.82	0.17	58.82	0.17
R, G, DVI, MCARI1	100	1	94.12	0.88	100	1	100	1	88.24	0.76	76.47	0.53	52.94	0.06	52.94	0.06
RGB	76.47	0.52	58.82	0.17	82.35	0.65	76.47	0.53	64.71	0.30	58.82	0.19	94.12	0.88	94.12	0.88
Indices	76.47	0.52	64.71	0.28	82.35	0.65	82.35	0.65	70.58	0.41	58.82	0.20	88.24	0.76	88.24	0.76
RGB and indices	76.47	0.52	76.47	0.52	82.35	0.65	76.47	0.53	70.59	0.41	58.82	0.20	94.12	0.88	88.24	0.76
R, G, NGRDI, GLI, TGI	76.47	0.52	76.47	0.52	82.35	0.65	82.35	0.65	82.35	0.65	58.82	0.20	88.24	0.76	82.35	0.64
G, B, CRI1, PRI	70.59	0.40	70.59	0.40	82.35	0.65	64.71	0.28	70.59	0.42	58.82	0.19	88.24	0.76	88.24	0.76
Agronomic parameters	88.24	0.77	82.35	0.65	94.12	0.88	94.12	0.88	82.35	0.65	88.24	0.77	64.71	0.28	58.82	0.17

Subsets classified	20 DAI				24 DAI				28 DAI			
	SVM		NB		SVM		NB		SVM		NB	
	OA	K	OA	K	OA	K	OA	K	OA	K	OA	K
RGN	76.47	0.53	76.47	0.53	100	1	100	1	64.71	0.31	58.82	0.19
Indices	47.06	-0.06	47.06	-0.04	94.12	0.88	88.24	0.76	47.06	-0.04	58.82	0.20
RGN and indices	76.47	0.53	76.47	0.53	100	1	100	1	47.06	-0.06	58.82	0.20
R, N, NDVI, SR, GNDVI	76.47	0.53	76.47	0.53	100	1	100	1	47.06	-0.06	58.82	0.20
R, G, DVI, MCARI1	76.47	0.53	76.47	0.53	100	1	100	1	52.94	0.07	58.82	0.19
RGB	100	1	94.12	0.88	100	1	100	1	29.41	-0.42	29.41	-0.44
Indices	100	1	82.35	0.64	82.35	0.64	100	1	35.29	-0.29	35.29	-0.29
RGB and indices	100	1	82.24	0.76	100	1	100	1	41.18	-0.18	41.18	-0.18
R, G, NGRDI, GLI, TGI	88.24	0.77	94.12	0.88	100	1	100	1	41.18	-0.18	41.18	-0.18
G, B, CRI1, PRI	100	1	88.24	0.76	100	1	94.12	0.88	35.29	-0.31	35.29	-0.33
Agronomic parameters	82.35	0.64	82.35	0.64	88.24	0.76	88.24	0.76	76.47	0.53	70.59	0.41

DAI: Days after inoculation; SVM: Support Vector Machine; NB: Naive Bayes; OA: Overall Accuracy; K: Kappa Index.

because pigment-related symptoms were not yet visible (Table 2).

At 16 DAI, infected plants showed greater reflectance in the red band (52.77) and less in the NIR band (50.97). However, the difference in the red band reflectance between healthy and infected plants was around 30% greater than that observed at 8 DAI (Figure 3), demonstrating its relationship with plant pigmentation.

The difference in reflectance between healthy and infected plants for the NIR band was 240% lower at 16 DAI than at 8 DAI (Figure 3), indicating a weaker relationship with cell structure.

At 16 DAI, plants showed visible symptoms of disease, which may explain why the multispectral sensor generally produced lower overall accuracy and Kappa coefficient values, and as such, the subsets obtained from the RGB showed the best performance (Table 2).

For the aforementioned assessment times, the stress caused by the bacteria resulted in a slight decline in most of the agronomic parameters evaluated. Lower average values were recorded for root length, plant fresh mass, stem diameter and chlorophyll content in infected plants at 8 DAI, and for the last three parameters at 16 DAI. Average fresh root mass was the same for both assessment times (Table 3).

Table 3. Mean values of agronomic parameters at 8 and 16 days after inoculation (DAI).

Agronomic parameters	8 DAI		16 DAI	
	Healthy	Infected	Healthy	Infected
Root length (cm)	24.91	23.61	16.25	29.09
Plant fresh mass (kg)	0.20	0.14	0.18	0.14
Fresh root mass (kg)	0.02	0.02	0.02	0.02
Stem diameter (mm)	15.22	13.42	15.90	13.88
Chlorophyll index	16.83	16.56	17.34	17.08

The radiometric data and agronomic parameters of healthy and infected plants were classified by two machine learning algorithms for all seven assessment times (Table 2). Based on classification, overall accuracy varied for the SVM and NB classifiers from 29.41 to 100%, and the Kappa coefficient from -0.42 to 1 for SVM and -0.44 to 1 for NB (Table 2).

At 4 DAI, the SVM classifier obtained 100% overall accuracy and a Kappa coefficient of 1 for the subsets RGN and indices; R, N, NDVI, SR and GNDVI; and R, G, DVI and MCARI1. For the NB classifier, the first two subsets also exhibited 100% overall accuracy and a Kappa coefficient of 1, that is, perfect agreement (Wang et al. 2020b), demonstrating the ability to differentiate between healthy and infected plants. The remaining multispectral subsets displayed almost perfect agreement ($k = 0.88$), except for RGN bands.

The visible sensor subsets showed slight ($k=0.17$) to moderate agreement ($k=0.52$) and the agronomic parameters substantial agreement ($k=0.77$ and 0.65 for the SVM and NB classifiers, respectively) (Wang et al. 2020b) (Table 2).

At 8 DAI, the subsets RGN and indices; R, G, DVI and MCARI1; and RGN bands obtained by the SVM classifier showed 100% accuracy ($k=1$), which was also observed for the last two subsets with the NB algorithm (Table 2). The remaining multispectral subsets obtained substantial ($k=0.64$ and 0.76) and almost perfect agreement ($k=0.88$). Most of the visible sensor subsets demonstrated substantial agreement ($k=0.65$) and the agronomic parameters almost perfect agreement ($k=0.88$) (Table 2).

At 12 DAI, accuracy and the Kappa coefficient declined for both classifiers in the multispectral and visible sensor subsets. Among the multispectral subsets, only the RGN ($k=0.65$) and R, G, DVI and MCARI1 bands ($k=0.76$) obtained with the SVM classifier and the visible sensor subsets R, G, NGRDI, GLI and TGI ($k=0.65$) exhibited substantial agreement ($k=0.61$ a 0.8) (Wang et al. 2020b), also observed for the agronomic parameters (Table 2).

The global accuracy and Kappa values of the multispectral subsets for both SVM and NB were lower at 16 DAI ($k=0.05$ – 0.29) than 12 DAI, unlike those of the visible sensor subsets, which increased significantly at 16 DAI. This could be because lesions were larger than 10 mm at this time, affecting leaves close to the inoculation site, which may have increased overall accuracy and Kappa values (Table 2).

The best classifications at 16 DAI were for RGB bands and; RGB and indices obtained by SVM, with $k=0.88$ (almost perfect agreement), RGB bands for the NB classifier (Table 2), although the remaining subsets showed substantial agreement ($k=0.61$ – 0.8). Classification of the agronomic parameters showed fair agreement ($k=0.28$) for SVM and slight ($k=0.17$) for NB (Wang et al. 2020b), that is, worse classification than that of the remaining intervals.

At 20 DAI, RGB bands; indices; RGB and indices; and G, B, CRI1 and PRI classifier exhibited 100% overall accuracy and $k=1$ (perfect agreement) for the SVM classifier, but substantial and almost perfect agreement for the NB algorithm (Table 2). By contrast, most of the multispectral subsets displayed moderate agreement ($k=0.53$) and the agronomic parameters substantial agreement ($k=0.64$).

In general, the best results were recorded at 24 DAI for both the multispectral and visible sensors. With the exception of the subset of multispectral

indices, the remainder, by one or both classifiers, obtained 100% overall accuracy ($k=1$), corresponding to perfect agreement (Wang et al. 2020b), whereas the agronomic parameters showed substantial agreement ($k=0.76$) (Table 2).

Finally, Kappa coefficients below zero were more common at 28 DAI, that is, poor agreement, while agronomic parameters performed better and exhibited moderate agreement ($k=0.41$ – 0.6) (Wang et al. 2020b).

Discussion

Some multispectral subsets enabled early detection of disease (at 4 and 8 DAI), using both classifiers (Table 2). This occurred before the characteristic symptoms of the disease were visible and without the need to destroy the plants, or, in the case of visual symptoms, present at 16 DAI, when the lesions caused by the bacteria were larger than 10 mm and had reached the leaves near the inoculation site. This demonstrates that although the disease is invisible to the naked eye, the presence of the bacteria can cause physiological changes that alter the plant's reflectance, which provided good classification results at the first and second assessment.

This corroborates the findings of West et al. (2010), who reported that plant diseases can cause physiological modifications in the rate of transpiration, leaf shape and color, as well as changes in canopy morphology and density (West et al. 2010), thereby altering plant reflectance and allowing faster disease classification using multispectral images. In the present study, this change was due to the action of pectinolytic enzymes (pectinases) produced by pathogen. These enzymes degrade the pectic substances present mainly in the middle lamella, resulting in separation and death of cells, that is tissue maceration and, therefore in the destruction of structural integrity (Pascholati and Dalio 2018).

At 4 DAI, classifications of RGN and indices; R, N, NDVI, SR and GNDVI and; R, G, DVI and MCARI1 showed 100% overall accuracy ($k=1$) (Table 2), that is, early detection of disease. Abdollahi et al. (2004) reported a decline in chlorophyll a and b content 42 h after in vitro inoculation of pear shoots with *Erwinia amylovora*. However, early detection related to changes in plant pigmentation is less common, so much so that at 4 DAI, classifications obtained with the visible sensor (RGB) were less accurate than those of the multispectral sensor. In other words, pigments sensitive to the visible spectrum were not yet decisive in distinguishing between the cell structure of healthy and infected plants (Table 2).

Thus, vegetation indices may be more correlated with biomass than simply red and near-infrared measurements (Jensen 2016). Combining bands and indices (Table 2) with their previously studied applications (Table 1) may have contributed to the superior performance of the classifiers at 4 DAI for the multispectral camera (Table 2).

The RGN bands, RGN and indices; and R, G, DVI, MCARI1 subset achieved 100% ($k=1$) overall accuracy at 8 DAI (Table 2). In infected plants, mean spectra of the red and green bands increased and the NIR band decreased (Figure 3). This corroborates the findings of Ren et al. (2017), who observed an increase in the blue, green and red intervals of typical reflectance spectra for unhealthy lettuce, as well as a sharp decline in the NIR band.

Sandmann et al. (2018) studied lettuce seedlings inoculated with *Rhizoctonia solani* and also obtained a higher average value for the red band and lower for the NIR band, as observed in the present study at 8 DAI (Figure 3).

Although the average root fresh mass of healthy and infected plants was the same in our study (Table 3), Osco et al. (2019) found that the root dry weight of lettuce plants showed the highest correlation with the NIR interval.

Bagheri (2020) used UAVs to detect pear trees infected with *Erwinia amylovora* and considered the NIR, red and green bands adequate; however, since there are no visible symptoms in the first stage of infection, the NIR band can be used for early detection because the internal structure of the leaf alters light absorption. Similarly, Chen et al. (2020) reported that spectral data in the NIR interval can help identify peanut plants in the early stages of bacterial wilt (*Ralstonia solanacearum*), when the xylem is slightly affected while the leaves are still green. Thus, based on infrared reflectance, the results obtained at 8 DAI are believed to be more reliable for differentiating between healthy and infected plants (Table 2).

The vegetation indices obtained with the multispectral sensor (NDVI, DVI, GNDVI, SR and MCARI1) also contributed to detecting the presence or absence of disease in plants (Table 1). This corroborates the findings of Sandmann et al. (2018), who recorded a lower average NDVI value for infected lettuce seedlings when compared to their healthy counterparts, and those of other studies, which demonstrated that these indices are also related to plant diseases (Fletcher et al. 2004; Cao et al. 2013; Zhang et al. 2018; Bagheri 2020; Abdulridha et al. 2020).

Accuracy and Kappa values declined at 12 DAI for both sensors (Table 2), indicating that 8 DAI is the cutoff point for early detection.

At 16 DAI, despite the difference in NIR bands between healthy and infected plants (Figure 3), most of the subsets exhibited slight agreement (Table 2), possibly because the high data variability confounded classification. At the onset of symptoms, the visible sensor was better able to distinguish between the two conditions, exhibiting substantial and almost perfect agreement (Table 2).

With respect to agronomic parameters, most related to cell structure, performed worst at 16 DAI ($k=0.17$ and 0.28), as observed for the multispectral sensor at the same assessment time (Table 2). However, at 4 and 8 DAI, agronomic parameters provided better overall accuracy and Kappa values, in particular at 8 DAI exhibiting almost perfect agreement ($k=0.88$) (Table 2), further demonstrating that cell structure is decisive in early disease detection.

At 16 DAI, the RGB bands and RGB and indices obtained the best classifications (Table 2). Similarly, Chávez et al. (2012) reported that the visible interval, particularly the blue and red bands, was capable of detecting the initial symptoms of bacterial wilt caused by *Ralstonia solanacearum* in potato plants. Thus, at this stage, pigments may be more important than cell structure in differentiating between infected and healthy plants.

Osco et al. (2019) found the highest negative and positive correlations in the red and blue bands, that is, the spectral bands for chlorophyll a and b absorption. In the present study, there was a slight decline in chlorophyll content, plant fresh mass and stem diameter between healthy and infected plants at 16 DAI (Table 3).

At 20 and 24 DAI, the visible sensor subsets also stood out (OA = 100%, $k=1$), whether using bands and indices alone or combined (Table 2). Odabas et al. (2017) found that using RGB components in a trained model made it possible to accurately estimate chlorophyll content in lettuce leaves.

The indices obtained with the visible sensor, related to chlorophyll, biomass, carotenoid content and photosynthetic efficiency (Table 1), and also involved in studies on plant diseases (Huang et al. 2007; Sapate and Deshmukh 2019; Sancho-Adamson et al. 2019; Bhandari et al. 2020), are believed to have contributed to the good results observed at 20 and 24 DAI. The combination of vegetation indices, based on different wavelengths that describe different physiological

parameters, increase the information content for automatic classification and improve its accuracy (Rumpf et al. 2010).

Thus, at 4, 8, 20 and 24 DAI, based on the subsets classified at 100% (Table 2) with perfect agreement and according to Wang et al. (2020b), the SVM classifier was accurate at distinguishing between healthy and infected plants. These data corroborate those obtained by other authors, who also reported high accuracy in classifying healthy and sick plants and leaves using the SVM classifier (Garcia-Ruiz et al. 2013; Abu-Khalaf and Salman 2013). For the NB classifier, maximum overall accuracy and $k=1$ were also recorded at 4, 8 and 24 DAI (Table 2), establishing the capacity of the algorithm. It is important to note that both classifiers provided a larger number of correct classifications at 24 DAI. As observed here, Karadag et al. (2018) found that the NB algorithm was able to differentiate between healthy and sick plants. This classifier also makes it possible to distinguish between disease classes (Mondal et al. 2017).

The worst results were observed at 28 DAI (Table 2). The pathogen inoculated is a root disease that did not manifest intensively in the aerial plants part this study, which may explain the varying spectral responses in the plants over time, making accurate classification more difficult. This was also expected by Bienkowski et al. (2019), who obtained considerably lower R^2 values when potato plants inoculated with *Pectobacterium atrosepticum* were compared to those inoculated with *Phytophthora infestans* and agreed that the former pathogen acts indirectly on leaves. Nevertheless, the authors were able to differentiate between the spectra of healthy and pre-symptomatic leaves and those with symptoms caused by *Pectobacterium atrosepticum*, with 74.6% classification accuracy (Bienkowski et al. 2019).

Conclusion

The results confirmed the possibility of pre-symptomatic detection of *Pectobacterium carotovorum* subsp. *carotovorum* in lettuce at 4 and 8 DAI, especially when using different subsets obtained by the multi-spectral sensor with SVM and NB classifiers before visible symptom onset in the field (16 DAI).

The best differentiation results were obtained at 20 (by SVM classifier) and 24 DAI (by SVM and NB classifier) with the conventional visible sensor.

This study presented a relatively simple method for detecting disease that can be applied in the field. The spectral reflectance of lettuce shows potential in

identifying soft rot caused by *Pectobacterium carotovorum* subsp. *carotovorum* and machine learning may be suitable for processing radiometric data and agronomic parameters.

Disclosure statement

No potential conflict of interest was reported by the author(s).

Funding

The authors are grateful to the Graduate Program in Agriculture and Geospatial Information of the Federal University of Uberlândia, Monte Carmelo Campus, and the Vegetable Crop Research Center (NUPOL) for their support, as well as the Coordination for the Improvement of Higher Education Personnel (CAPES) for the research grants awarded.

ORCID

Glecia Júnia dos Santos Carmo  <http://orcid.org/0000-0001-9476-8309>

Renata Castoldi  <http://orcid.org/0000-0001-9406-0917>
George Deroco Martins  <http://orcid.org/0000-0001-9738-7325>

Ana Carolina Pires Jacinto  <http://orcid.org/0000-0001-8184-5803>

Nilvanira Donizete Tebaldi  <http://orcid.org/0000-0001-6983-9718>

Hamilton César de Oliveira Charlo  <http://orcid.org/0000-0003-0663-2167>

Renan Zampiroli  <http://orcid.org/0000-0002-5082-9111>

Data availability statement

The datasets generated and/or analyzed during the present study are available from the corresponding author on reasonable request.

References

- Abdollahi, H., Rugini, E., Ruzzi, M., and Muleo, R. 2004. "In vitrosystem for studying the interaction between *Erwinia amylovora* and genotypes of pear." *Plant Cell, Tissue and Organ Culture*, Vol. 79(No. 2):pp. 203–212. doi:10.1007/s11240-004-0661-0.
- Abdu, A.M., Mokji, M.M., and Sheikh, U.U. 2020. "Automatic vegetable disease identification approach using individual lesion features." *Computers and Electronics in Agriculture*, Vol. 176: pp. 105660. doi:10.1016/j.compag.2020.105660.
- Abdulridha, J., Ampatzidis, Y., Roberts, P., and Kakarla, S.C. 2020. "Detecting powdery mildew disease in squash at different stages using UAV-based hyperspectral imaging and artificial intelligence." *Biosystems Engineering*,

- Vol. 197: pp. 135–148. doi:10.1016/j.biosystemseng.2020.07.001.
- Abu-Khalaf, N., and Salman, M. 2013. “Detecting plant diseases using visible/near infrared spectroscopy.” *NIR News*, Vol. 24 (No. 4):pp. 12–25. doi:10.1255/nirn.1369.
- Agrofit 2020. Sistemas de agrotóxicos fitossanitários. Accessed July 27 http://extranet.agricultura.gov.br/agrofit_cons/principal_agrofit_cons/
- Anuário Brasileiro de Horti&Fruti 2020 2019. Santa Cruz do Sul: Editora Gazeta Santa Cruz.
- Bagheri, N. 2020. “Application of aerial remote sensing technology for detection of fire blight infected pear trees.” *Computers and Electronics in Agriculture*, Vol. 168: pp. 105147. doi:10.1016/j.compag.2019.105147.
- Ballesteros, R., Ortega, J.F., Hernandez, D., Del Campo, A., and Moreno, M.A. 2018. “Combined use of agro-climatic and very high-resolution remote sensing information for crop monitoring.” *International Journal of Applied Earth Observation and Geoinformation*, Vol. 72: pp. 66–75. doi:10.1016/j.jag.2018.05.019.
- Berrar, D. P. 2018. “Bayes’ theorem and Naive Bayes classifier.” In *Encyclopedia of Bioinformatics and Computational Biology*, edited by Ranganathan S., K. Nakai and C. Schonbach, pp. 403–412. Amsterdam; Oxford; Cambridge: Elsevier.
- Bhandari, M., Ibrahim, A.M.H., Xue, Q., Jung, J., Chang, A., Rudd, J.C., Maeda, M., Rajan, N., Neely, H., and Landivar, J. 2020. “Assessing winter wheat foliage disease severity using aerial imagery acquired from small Unmanned Aerial Vehicle (UAV).” *Computers and Electronics in Agriculture*, Vol. 176 (No. No.6):p. 105665. doi:10.1016/j.compag.2020.105665.
- Bienkowski, D., Aitkenhead, M.J., Lees, A.K., Gallagher, C., and Neilson, R. 2019. “Detection and differentiation between potato (*Solanum tuberosum*) diseases using calibration models trained with non-imaging spectrometry data.” *Computers and Electronics in Agriculture*, Vol. 167: p. 105056. doi:10.1016/j.compag.2019.105056.
- Cao, X., Luo, Y., Zhou, Y., Duan, X., and Cheng, D. 2013. “Detection of powdery mildew in two winter wheat cultivars using canopy hyperspectral reflectance.” *Crop Protection*, Vol. 45: p. 124–131. doi:10.1016/j.cropro.2012.12.002.
- Chávez, P., Yarlequé, C., Loayza, H., Mares, V., Hanco, P., Priou, S., Márquez, M., et al. 2012. “Detection of bacterial wilt infection caused by *Ralstonia solanacearum* in potato (*Solanum tuberosum* L.) through multifractal analysis applied to remotely sensed data.” *Precision Agriculture*, Vol. 13 (No. 2):p. 236–255. doi:10.1007/s11119-011-9242-5.
- Chen, T., Yang, W., Zhang, H., Zhu, B., Zeng, R., Wang, X., Wang, S., et al. 2020. “Early detection of bacterial wilt in peanut plants through leaf-level hyperspectral and unmanned aerial vehicle data.” *Computers and Electronics in Agriculture*, Vol. 177 (No. 105708):p. 105708. doi:10.1016/j.compag.2020.105708.
- Colariccio, A., and Chaves, A. L. R. 2017. *Aspectos Fitossanitários da Cultura da Alface*. 29th ed. São Paulo: Instituto Biológico.
- Cortes, C., and Vapnik, V. 1995. “Support vector networks.” *Machine Learning*, Vol. 20 (No. 3):pp. 273–297. doi:10.1007/BF00994018.
- Díaz, B.M., and Blackburn, G.A. 2003. “Remote sensing of mangrove biophysical properties: Evidence from a laboratory simulation of the possible effects of background variation on spectral vegetation indices.” *International Journal of Remote Sensing*, Vol. 24 (No. 1):pp. 53–73. doi:10.1080/01431160305012.
- Embrapa – Empresa Brasileira de Pesquisa Agropecuária. 2006. *Sistema brasileiro de classificação de solos*. 2nd ed. Rio de Janeiro: Embrapa Solos.
- Félix, K.C.S., Oliveira, W.J., Mariano, R.L.R., and Souza, E.B. 2014. “Lettuce genotype resistance to “soft rot” caused by *Pectobacterium carotovorum* subsp. *carotovorum*.” *Scientia Agricola*, Vol. 71 (No. 4):pp. 287–291. doi:10.1590/0103-9016-2013-0301.
- Fernández, C.I., Leblon, B., Haddadi, A., Wang, K., and Wang, J. 2020. “Potato Late Blight Detection at the Leaf and Canopy Levels Based in the Red and Red-Edge Spectral Regions.” *Remote Sensing*, Vol. 12 (No. 8):p. 1292.
- Fletcher, R.S., Escobar, D.E., and Skaria, M. 2004. “Technical Note: Response of ratio vegetation indices to foot rot-infected citrus trees.” *International Journal of Remote Sensing*, Vol. 25 (No. 19):pp. 3967–3972. doi:10.1080/01431160310001652367.
- Fontes, P. C. R. 1999. “Alface.” In *Recomendações para o uso de corretivos e fertilizantes em Minas Gerais: 5º aproximação*, edited by A. C. Ribeiro, P. T. G. Guimarães, and V. H. A. Alvarez, p. 177. Viçosa: Sociedade Brasileira de Ciência do Solo.
- Gamon, J.A., Penuelas, J., and Field, C.B. 1992. “A narrow-waveband spectral index that tracks diurnal changes in photosynthetic efficiency.” *Remote Sensing of Environment*, Vol. 41 (No. 1):pp. 35–44. (No doi:10.1016/0034-4257(92)90059-S.
- Gao, H., Mao, H., and Zhang, X. 2015. “Determination of lettuce nitrogen content using spectroscopy with efficient wavelength selection and extreme learning machine.” *Zemdirbyste-Agriculture*, Vol. 102 (No. 1):pp. 51–58. doi:10.13080/z-a.2015.102.006.
- Garbulsky, M.F., Peñuelas, J., Gamon, J., Inoue, Y., and Filella, I. 2011. “The photochemical reflectance index (PRI) and the remote sensing of leaf, canopy and ecosystem radiation use efficiencies. A review and meta-analysis.” *Remote Sensing of Environment*, Vol. 115 (No. 2):pp. 281–297. doi:10.1016/j.rse.2010.08.023.
- García-Ruiz, F., Sankaran, S., Maja, J.M., Lee, W.S., Rasmussen, J., and Ehsani, R. 2013. “Comparison of two aerial imaging platforms for identification of Huanglongbing-infected citrus trees.” *Computers and Electronics in Agriculture*, Vol. 91: pp. 106–115. doi:10.1016/j.compag.2012.12.002.
- Gitelson, A.A., Kaufman, Y.J., and Merzlyak, M.N. 1996. “Use of a channel in remote sensing of global vegetation from EOS-MODIS.” *Remote Sensing of Environment*, Vol. 58 (No. 3):pp. 289–298. (No doi:10.1016/S0034-4257(96)00072-7.
- Gitelson, A.A., Zur, Y., Chivkunova, O.B., and Merzlyak, M.N. 2002. “Assessing Carotenoid Content in Plant Leaves with Reflectance Spectroscopy.” *Photochemistry and Photobiology*, Vol. 75 (No. 3):pp. 272–281. doi:10.1562/0031-8655(2002)075<0272:ACCIPL > 2.0.CO;2.

- Gogoi, N.K., Deka, B., and Bora, L.C. 2018. "Remote sensing and its use in detection and monitoring plant diseases: A review." *Agricultural Reviews*, Vol. 39 (No. 4):pp. 307–313.
- Gold, K.M., Townsend, P.A., Herrmann, I., and Gevens, A.J. 2020. "Investigating potato late blight physiological differences across potato cultivars with spectroscopy and machine learning." *Plant Science : An International Journal of Experimental Plant Biology*, Vol. 295: pp. 110316. doi:10.1016/j.plantsci.2019.110316.
- Haboudane, D., Miller, J.R., Pattey, E., Zarco-Tejada, P.J., and Strachan, I.B. 2004. "Hyperspectral vegetation indices and novel algorithms for predicting green LAI of crop canopies: Modeling and validation in the context of precision agriculture." *Remote Sensing of Environment*, Vol. 90 (No. 3):pp. 337–352. doi:10.1016/j.rse.2003.12.013.
- Hall, F.G., Strebe, D.E., Nickeson, J.E., and Goetz, S.J. 1991. "Radiometric rectification: Toward a common radiometric response among multirate, multisensor images." *Remote Sensing of Environment*, Vol. 35 (No. 1):pp. 11–27. doi:10.1016/0034-4257(91)90062-B.
- Hatfield, J.L., Gitelson, A.A., Schepers, J.S., and Walthall, C.L. 2008. "Application of spectral remote sensing for agronomic decisions." *Agronomy Journal*, Vol. 100 (No. S3):pp. S-117–S-131. doi:10.2134/agronj2006.0370c.
- Hetzroni, A., Miles, G.E., Engel, B.A., Hammer, P.A., and Latin, R.X. 1994. "Machine vision monitoring of plant health." *Advances in Space Research : The Official Journal of the Committee on Space Research (Cospar)*, Vol. 14 (No. 11):pp. 203–212. doi:10.1016/0273-1177(94)90298-4.
- Huang, W., Lamb, D.W., Niu, Z., Zhang, Y., Liu, L., and Wang, J. 2007. "Identification of yellow rust in wheat using in-situ spectral reflectance measurements and airborne hyperspectral imaging." *Precision Agriculture*, Vol. 8 (No. 4–5):pp. 187–197. doi:10.1007/s11119-007-9038-9.
- Hunt, E.R., Jr, Cavigelli, M., Daughtry, C.S.T., McMurtrey, J.E., and Walthall, C.L. 2005. "Evaluation of digital photography from model aircraft for remote sensing of crop biomass and nitrogen status." *Precision Agriculture*, Vol. 6 (No. 4):pp. 359–378. doi:10.1007/s11119-005-2324-5.
- Hunt, E.R., Jr, Daughtry, C.S.T., Eitel, J.U., and Long, D.S. 2011. "Remote sensing leaf chlorophyll content using a visible band index." *Agronomy Journal*, Vol. 103 (No. 4): pp. 1090–1099. doi:10.2134/agronj2010.0395.
- Hunt, E.R., Jr, Hively, W.D., Fujikawa, S., Linden, D., Daughtry, C.S.T., and McCarty, G. 2010. "Acquisition of NIR-Green-Blue Digital Photographs from Unmanned Aircraft for Crop Monitoring." *Remote Sensing*, Vol. 2 (No. 1):pp. 290–305. doi:10.3390/rs2010290.
- Jensen, J. R. 2016. *Introductory digital image processing: a remote sensing perspective*. 4th ed. Glenview, IL: Pearson Education.
- Jordan, C.F. 1969. "Derivation of leaf-area index from quality of light on the forest floor." *Ecology*, Vol. 50 (No. 4): pp. 663–666. doi:10.2307/1936256.
- Jun, S., Xiaming, J., Hanping, M., Xiaohong, W., Hongyan, G., Wenjing, Z., and Xiao, L. 2013. "Detecting nitrogen content in lettuce leaves based on hyperspectral imaging and multiple regression analysis." *Information Technology Journal*, Vol. 12 (No. 19):pp. 4845–4851. doi:10.3923/ijt.2013.4845.4851.
- Kado, C.I., and Heskett, M.G. 1970. "Selective media for isolation of *Agrobacterium*, *Corynebacterium*, *Erwinia*, *Pseudomonas*, and *Xanthomonas*." *Phytopathology*, Vol. 60 (No. 6):pp. 969–976. doi:10.1094/phyto-60-969.
- Karadag, K., Tenekeci, M. E., Taşaltın, R., and Bilgili, A. 2018. *Detection of pepper fusarium disease using machine learning algorithms based on spectral reflectance*. Sustainable Computing: Informatics and Systems. Advance online publication. doi:10.1016/j.suscom.2019.01.001.
- Kizil, Ü., Genç, L., İnalpulat, M., Sapolyo, D., and Mirik, M. 2012. "Lettuce (*Lactuca sativa* L.) yield prediction under water stress using artificial neural network (ANN) model and vegetation indices." *Žemdirbystė Agriculture*, Vol. 99 (No. 4):pp. 409–418.
- Liakos, K., Busato, P., Moshou, D., Pearson, S., and Bochtis, D. 2018. "Machine learning in agriculture: A review." *Sensors*, Vol. 18 (No. 8):pp. 2674. doi:10.3390/s18082674.
- Louhaichi, M., Borman, M.M., and Johnson, D.E. 2001. "Spatially located platform and aerial photography for documentation of grazing impacts on wheat." *Geocarto International*, Vol. 16 (No. 1):pp. 65–70. doi:10.1080/10106040108542184.
- Maes, W.H., and Steppe, K. 2019. "Perspectives for remote sensing with unmanned aerial vehicles in precision agriculture." *Trends in Plant Science*, Vol. 24 (No. 2):pp. 152–164. doi:10.1016/j.tplants.2018.11.007.
- Mahlein, A.-K. 2016. "Plant disease detection by imaging sensors - parallels and specific demands for precision agriculture and plant phenotyping." *Plant Disease*, Vol. 100 (No. 2):pp. 241–251. doi:10.1094/PDIS-03-15-0340-FE.
- Mansfield, J.O.H.N., Genin, S., Magori, S., Citovsky, V., Sriariyanum, M., Ronald, P., Dow, M.A.X., et al. 2012. "Top 10 plant pathogenic bacteria in molecular plant pathology." *Molecular Plant Pathology*, Vol. 13 (No. 6): pp. 614–629. doi:10.1111/j.1364-3703.2012.00804.x.
- Mao, H., Gao, H., Zhang, X., and Kumi, F. 2015. "Nondestructive measurement of total nitrogen in lettuce by integrating spectroscopy and computer vision." *Scientia Horticulturae*, Vol. 184: pp. 1–7. doi:10.1016/j.scienta.2014.12.027.
- Mckinnon, T., and Hoff, P. 2017. "Comparing RGB-based vegetation indices with NDVI for drone based agricultural sensing." *Agribotix, LLC*, pp. 1–8.
- Moges, S.M., Raun, W.R., Mullen, R.W., Freeman, K.W., Johnson, G.V., and Solie, J.B. 2005. "Evaluation of green, red, and near infrared bands for predicting winter wheat biomass, nitrogen uptake, and final grain yield." *Journal of Plant Nutrition*, Vol. 27 (No. 8):pp. 1431–1441. doi:10.1081/PLN-200025858.
- Mondal, D., Kole, D.K., and Roy, K. 2017. "Gradation of yellow mosaic virus disease of okra and bitter gourd based on entropy based binning and Naive Bayes classifier after identification of leaves." *Computers and Electronics in Agriculture*, Vol. 142: pp. 485–493. doi:10.1016/j.compag.2017.11.024.
- Morellos, A., Tziotzios, G., Orfanidou, C., Pantazi, X.E., Sarantaris, C., Maliogka, V., Alexandridis, T.K., and Moshou, D. 2020. "Non-destructive early detection and quantitative severity stage classification of *Tomato Chlorosis Virus* (ToCV) infection in young tomato plants

- using vis-NIR Spectroscopy.” *Remote Sensing*, Vol. 12 (No. 12):p. 1920. doi:10.3390/rs12121920.
- Mountrakis, G., Im, J., and Ogole, C. 2011. “Support vector machines in remote sensing: A review.” *ISPRS Journal of Photogrammetry and Remote Sensing*, Vol. 66 (No. 3):pp. 247–259. doi:10.1016/j.isprsjprs.2010.11.001.
- Nazerian, E., Sijam, K., Ahmad, Z.A.M., and Vadamalai, G. 2013. “Characterization of *Pectobacterium carotovorum* subsp. *carotovorum* as a new disease on Lettuce in Malaysia.” *Australasian Plant Disease Notes*, Vol. 8 (No. 1):pp. 105–107. doi:10.1007/s13314-013-0107-9.
- Odabas, M.S., Simsek, H., Lee, C.W., and İseri, İ. 2017. “Multilayer perceptron neural network approach to estimate chlorophyll concentration index of lettuce (*Lactuca sativa* L.).” *Communications in Soil Science and Plant Analysis*, Vol. 48 (No. 2):pp. 162–169.
- Oerke, E.C. 2020. “Remote Sensing of Diseases.” *Annual Review of Phytopathology*, Vol. 58: pp. 225–252. doi:10.1146/annurev-phyto-010820-012832.
- Oscó, L.P., Ramos, A.P.M., Moriya, É.A.S., Bavaresco, L.G., Lima, B. C. d., Estrabis, N., Pereira, D.R., et al. 2019. “Modeling hyperspectral response of water-stress induced lettuce plants using artificial neural networks.” *Remote Sensing*, Vol. 11 (No. 23):p. 2797. doi:10.3390/rs11232797.
- Ozguven, M.M., and Adem, K. 2019. “Automatic detection and classification of leaf spot disease in sugar beet using deep learning algorithms.” *Physica A: Statistical Mechanics and Its Applications*, Vol. 535: p. 122537. doi:10.1016/j.physa.2019.122537.
- Pascholati, S. F., and Dalio, R. J. D. 2018. “Fisiologia do Parasitismo: Como os patógenos atacam as plantas.” In *Manual de Fitopatologia: Princípios e Conceitos*, edited by L. Amorim, J.A.M. Rezende, and A. Bergamin Filho, pp. 319–419. Ouro Fino: Editora Agronômica Ceres.
- Pineda, M., Pérez-Bueno, M.L., and Barón, M. 2018. “Detection of bacterial infection in melon plants by classification methods based on imaging data.” *Frontiers in Plant Science*, Vol. 9: p. 164. doi:10.3389/fpls.2018.00164.
- Poblete, T., Camino, C., Beck, P.S.A., Hornero, A., Kattenborn, T., Saponari, M., Boscia, D., Navas-Cortes, J.A., and Zarco-Tejada, P.J. 2020. “Detection of *Xylella fastidiosa* infection symptoms with airborne multispectral and thermal imagery: Assessing bandset reduction performance from hyperspectral analysis.” *ISPRS Journal of Photogrammetry and Remote Sensing*, Vol. 162: pp. 27–40. doi:10.1016/j.isprsjprs.2020.02.010.
- Ponzoni, F. J., Shimabukuro, Y. E., and Kuplich, T. M. 2012. *Sensoriamento Remoto da vegetação. 2nd ed. Atualizada e ampliada*. São Paulo: Oficina de Textos.
- Rahi, S., Mobli, H., Jamshidi, B., Azizi, A., and Sharifi, M. 2020. “Different supervised and unsupervised classification approaches based on visible/near infrared.” *Infrared Physics & Technology*, Vol. 108 (No. 1):p. 103355. doi:10.1016/j.infrared.2020.103355.
- Ren, D.D.W., Tripathi, S., and Li, L.K.B. 2017. “Low-cost multispectral imaging for remote sensing of lettuce health.” *Journal of Applied Remote Sensing*, Vol. 11 (No. 1):p. 016006. doi:10.1117/1.JRS.11.016006.
- Ren, J., Petzoldt, R., and Dickson, M.H. 2001. “Genetics and population improvement of resistance to bacterial soft rot Chinese cabbage.” *Euphytica*, Vol. 118 (No. 3):pp. 271–280. doi:10.1023/A:1017522501229.
- Rouse, W. J., Haas, R. H., Schell, J. A., and Deering, D. W. 1973. “Monitoring vegetation systems in the great plains with ERTS.” In *Third ERTS Symposium*, Proceedings, pp. 309–317. Washington, DC: NASA.
- Rumpf, T., Mahlein, A.-K., Steiner, U., Oerke, E.-C., Dehne, H.-W., and Plümer, L. 2010. “Early detection and classification of plant diseases with Support Vector Machines based on hyperspectral reflectance.” *Computers and Electronics in Agriculture*, Vol. 74 (No. 1):pp. 91–99. doi:10.1016/j.compag.2010.06.009.
- Sancho-Adamson, M., Trillas, M., Bort, J., Fernandez-Gallego, J., and Romanya, J. 2019. “Use of RGB vegetation indexes in assessing early effects of *Verticillium Wilt* of olive in asymptomatic plants in high and low fertility scenarios.” *Remote Sensing*, Vol. 11 (No. 6):p. 607. doi:10.3390/rs11060607.
- Sandmann, M., Grosch, R., and Graefe, J. 2018. “The use of features from fluorescence, thermography, and NDVI imaging to detect biotic stress in lettuce.” *Plant Disease*, Vol. 102 (No. 6):pp. 1101–1107. doi:10.1094/PDIS-10-17-1536-RE.
- Sapate, N.M., and Deshmukh, R.R. 2019. “Spectral and numerical analysis of hyper spectral data using vegetation indices.” *International Journal of Engineering and Advanced Technology*, Vol. 8 (No. 6):pp. 2249–8958.
- Starý, K., Jelínek, Z., Kumhálová, J., Chyba, J., and Balážová, K. 2020. “Comparing RGB - based vegetation indices from UAV imageries to estimate hops canopy area.” *Agronomy Research*, Vol. 18 (No. 4):pp. 2592–2601.
- Sun, J., Ge, X., Wu, X., Dai, C., and Yang, N. 2018. “Identification of pesticide residues in lettuce leaves based on near infrared transmission spectroscopy.” *Journal of Food Process Engineering*, Vol. 41:e12816. doi:10.1111/jfpe.12816.
- Tetila, E.C., Machado, B.B., Belete, N.A.S., Guimarães, D.A., and Pistori, H. 2017. “Identification of soybean foliar diseases using unmanned aerial vehicle images.” *IEEE Geoscience and Remote Sensing Letters*, Vol. 14 (No. 12): pp. 2190–2194. doi:10.1109/LGRS.2017.2743715.
- Tucker, C.J. 1979. “Red and photographic infrared linear combinations for monitoring vegetation.” *Remote Sensing of Environment*, Vol. 150 (No. 2):pp. 127–150.
- Usha, K., and Singh, B. 2013. “Potential applications of remote sensing in horticulture - a review.” *Scientia Horticulturae*, Vol. 153: pp. 71–83. doi:10.1016/j.scienta.2013.01.008.
- Wang, T., Thomasson, J.A., Yang, C., Isakeit, T., and Nichols, R.L. 2020a. “Automatic classification of cotton root rot disease based on UAV remote sensing.” *Remote Sensing*, Vol. 12 (No. 8):p. 1310. doi:10.3390/rs12081310.
- Wang, T., Thomasson, J.A., Isakeit, T., Yang, C., and Nichols, R.L. 2020b. “A plant-by-plant method to identify and treat cotton root rot based on UAV remote sensing.” *Remote Sensing*, Vol. 12 (No. 15):p. 2453. (Nodoi:10.3390/rs12152453).
- Weiss, M., Jacob, F., and Duveiller, G. 2020. “Remote sensing for agricultural applications: A meta-review.” *Remote Sensing of Environment*, Vol. 236: pp. 111402. doi:10.1016/j.rse.2019.111402.
- West, J. S., Bravo, C., Oberti, R., Moshou, D., Ramon, H., and McCartney, H. A. 2010. “Detection of fungal diseases optically and pathogen inoculum by air sampling.” In

- Precision Crop Protection - the Challenge and Use of Heterogeneity*, edited by E.C. Oerke, R. Gerhards, G. Menz, and R.A. Sikora, pp. 135–149. London: Springer Dordrecht Heidelberg.
- Wiegand, C.L., Richardson, A.J., Escobar, D.E., and Gerbermann, A.H. 1991. "Vegetation indices in crop assessments." *Remote Sensing of Environment*, Vol. 35 (No. 2–3): pp. 105–119. doi:10.1016/0034-4257(91)90004-P.
- Xin, Z., Jun, S., Yan, T., Quansheng, C., Xiaohong, W., and Yingying, H. 2020. "A deep learning based regression method on hyperspectral data for rapid prediction of cadmium residue in lettuce leaves." *Chemometrics and Intelligent Laboratory Systems*, Vol. 200: p. 103996. doi:10.1016/j.chemolab.2020.103996.
- Zarate-Valdez, J.L., Whiting, M.L., Lampinen, B.D., Metcalf, S., Ustin, S.L., and Brown, P.H. 2012. "Prediction of leaf area index in almonds by vegetation indexes." *Computers and Electronics in Agriculture*, Vol. 85: pp. 24–32. doi:10.1016/j.compag.2012.03.009.
- Zhang, D., Zhou, X., Zhang, J., Lan, Y., Xu, C., Liang, D., and Wang, Z. 2018. "Detection of rice sheath blight using an unmanned aerial system with high-resolution color and multispectral imaging." *Plos One*, Vol. 13 (No. 5):p. e0187470.